

University of Wollongong

Research Online

Faculty of Engineering and Information
Sciences - Papers: Part B

Faculty of Engineering and Information
Sciences

2020

State of charge estimation in lithium-ion batteries: A neural network optimization approach

M Hossain Lipu

M Hannan

Aini Hussain

Afida Ayob

Mohamad Saad

See next page for additional authors

Follow this and additional works at: <https://ro.uow.edu.au/eispapers1>



Part of the [Engineering Commons](#), and the [Science and Technology Studies Commons](#)

Recommended Citation

Hossain Lipu, M; Hannan, M; Hussain, Aini; Ayob, Afida; Saad, Mohamad; and Muttaqi, Kashem M., "State of charge estimation in lithium-ion batteries: A neural network optimization approach" (2020). *Faculty of Engineering and Information Sciences - Papers: Part B*. 4385.

<https://ro.uow.edu.au/eispapers1/4385>

Research Online is the open access institutional repository for the University of Wollongong. For further information contact the UOW Library: research-pubs@uow.edu.au

State of charge estimation in lithium-ion batteries: A neural network optimization approach

Abstract

© 2020, MDPI AG. All rights reserved. The development of an accurate and robust state-of-charge (SOC) estimation is crucial for the battery lifetime, efficiency, charge control, and safe driving of electric vehicles (EV). This paper proposes an enhanced data-driven method based on a time-delay neural network (TDNN) algorithm for state of charge (SOC) estimation in lithium-ion batteries. Nevertheless, SOC accuracy is subject to the suitable value of the hyperparameters selection of the TDNN algorithm. Hence, the TDNN algorithm is optimized by the improved firefly algorithm (iFA) to determine the optimal number of input time delay (UTD) and hidden neurons (HNs). This work investigates the performance of lithium nickel manganese cobalt oxide (LiNiMnCoO₂) and lithium nickel cobalt aluminum oxide (LiNiCoAlO₂) toward SOC estimation under two experimental test conditions: the static discharge test (SDT) and hybrid pulse power characterization (HPPC) test. Also, the accuracy of the proposed method is evaluated under different EV drive cycles and temperature settings. The results show that iFA-based TDNN achieves precise SOC estimation results with a root mean square error (RMSE) below 1%. Besides, the effectiveness and robustness of the proposed approach are validated against uncertainties including noise impacts and aging influences.

Disciplines

Engineering | Science and Technology Studies

Publication Details




M. Hossain Lipu, M. Hannan, A. Hussain, A. Ayob, M. Saad & K. Muttaqi, "State of charge estimation in lithium-ion batteries: A neural network optimization approach," *Electronics* (Switzerland), vol. 9, (9) pp. 1-24, 2020.

Authors

M Hossain Lipu, M Hannan, Aini Hussain, Afida Ayob, Mohamad Saad, and Kashem M. Muttaqi

Article

State of Charge Estimation in Lithium-Ion Batteries: A Neural Network Optimization Approach

M. S. Hossain Lipu ^{1,*}, M. A. Hannan ^{2,*}, Aini Hussain ¹, Afida Ayob ¹,
Mohamad H. M. Saad ³ and Kashem M. Muttaqi ⁴

¹ Department of Electrical, Electronic and Systems Engineering, Universiti Kebangsaan Malaysia, Bangi 43600, Malaysia; draini@ukm.edu.my (A.H.); afida.ayob@ukm.edu.my (A.A.)

² Department of Electrical Power Engineering, College of Engineering, Universiti Tenaga Nasional, Kajang 43000, Malaysia

³ Department of Mechanical and Manufacturing Engineering, Universiti Kebangsaan Malaysia, Bangi 43600, Malaysia; hanifsaad@ukm.edu.my

⁴ School of Electrical, Computer and Telecommunications Engineering, University of Wollongong, Wollongong, NSW 2522, Australia; kashem@uow.edu.au

* Correspondence: lipu@ukm.edu.my (M.S.H.L.); hannan@uniten.edu.my (M.A.H.)

Received: 1 August 2020; Accepted: 3 September 2020; Published: 22 September 2020



Abstract: The development of an accurate and robust state-of-charge (SOC) estimation is crucial for the battery lifetime, efficiency, charge control, and safe driving of electric vehicles (EV). This paper proposes an enhanced data-driven method based on a time-delay neural network (TDNN) algorithm for state of charge (SOC) estimation in lithium-ion batteries. Nevertheless, SOC accuracy is subject to the suitable value of the hyperparameters selection of the TDNN algorithm. Hence, the TDNN algorithm is optimized by the improved firefly algorithm (iFA) to determine the optimal number of input time delay (UTD) and hidden neurons (HNs). This work investigates the performance of lithium nickel manganese cobalt oxide (LiNiMnCoO₂) and lithium nickel cobalt aluminum oxide (LiNiCoAlO₂) toward SOC estimation under two experimental test conditions: the static discharge test (SDT) and hybrid pulse power characterization (HPPC) test. Also, the accuracy of the proposed method is evaluated under different EV drive cycles and temperature settings. The results show that iFA-based TDNN achieves precise SOC estimation results with a root mean square error (RMSE) below 1%. Besides, the effectiveness and robustness of the proposed approach are validated against uncertainties including noise impacts and aging influences.

Keywords: time-delay neural network; improved firefly algorithm; lithium-ion battery; state of charge; electric vehicle

1. Introduction

Environmental issues such as global warming, climate change, and carbon emissions drive the necessity to deploy battery storage technologies [1]. Lithium-ion batteries are extensively employed in the automotive industry due to their attractive characteristics such as low self-discharge, long life cycle, high voltage, and high energy density [2]. However, the lithium-ion battery has some issues such as performance degradation with aging cycles, temperature rise, accurate charge estimation, over-charging, and over-discharging [3]. Thus, further investigation is required on the lithium-ion battery charge estimation under a safe temperature region in electric vehicle (EV) applications.

EV has a battery management system (BMS) that executes operations such as state of charge (SOC) monitoring, battery health estimation, remaining life prediction, temperature management, battery equalization, and fault diagnosis [4,5]. SOC is a crucial parameter of BMS which defines the

residual charge existing inside a battery cell [6,7]. SOC in EV applications has become an increasingly popular research topic and is of great importance for improving battery lifecycles. An accurate SOC calculation technique confirms the safe driving operation and protects the battery from many abnormalities such as over-charged, over-discharged, and over-heating problems. Nonetheless, SO is influenced by various factors such as the cathode material, material degradation, aging cycles, and temperatures [8]. Hence, advanced research is concerned greatly with developing an accurate and robust SOC estimation algorithm.

1.1. Related Works

A lot of studies have reported different approaches for SOC estimation of lithium-ion batteries under different operating conditions. The conventional methods like coulomb counting (CC) [9] and open-circuit voltage (OCV) [10] are the straightforward approaches for estimating SOC. Nevertheless, the accuracy of the CC method is affected by sensor precision which accumulates during each current integration. The OCV method obtains SOC by looking up the OCV vs. SOC curve; nevertheless, it needs a long rest time and cannot operate in online conditions. To overcome these concerns, model-based SOC estimation methods have been proposed. The model-based methods utilize a battery model incorporated with adaptive filter algorithms such as the extended Kalman filter (EKF) [11], unscented Kalman filter (UKF) [12], particle filter (PF) [13], H-infinity filter [14] and sliding mode observer [15] to estimate SOC. The KF is a popular approach for SOC estimation; however, the accuracy of KF may diverge badly in a highly nonlinear system. PF has fast execution and can deliver accurate SOC results. Nevertheless, PF has a complex mathematical computation. The H-infinity filter is suitable for moderate accuracy and a low computational cost. However, the performance would abruptly decrease owing to temperature and aging effects. In recent years, data-driven SOC estimation approaches have gained a lot of attention around the world because of their robust computation capabilities for handling highly non-linear lithium-ion battery characteristics. Besides, data-driven approaches examine SOC without exploring battery material structure, features, and associated chemical reactions [16]. The back-propagation neural network (BPNN) algorithm offers simple and easy execution but suffers from slow training operation [17]. The radial basis function neural network (RBFNN) achieves reasonable SOC accuracy with incomplete information; however, it has the shortcoming of lengthy training duration [18]. The extreme learning machine (ELM) is excellent with regard to fast learning speed and improved generalization performance, but the accuracy is influenced by the number of hidden layer neurons [19]. Although the wavelet neural network (WNN) has less complexity in training operation, it needs many hidden units. The support vector machine (SVM) can estimate SOC in the highly non-linear system, but has a complex execution process [20]. Gaussian process regression (GPR) can estimate SOC with model uncertainty; nonetheless, it has a drawback of poor efficiency in high dimensional spaces [21]. The nonlinear autoregressive with exogenous input neural network (NARXNN) is effective for mapping the lithium-ion battery non-linear characteristics, but the performance highly depends on the suitable value of the hyperparameters [22]. The long short-term memory (LSTM) [23] and gated recurrent unit (GRU) [24] can examine SOC under long-term dependencies; however, they require a large pool of data and an appropriate training operation to achieve accurate SOC estimation results. The adaptive neuro-fuzzy inference system (ANFIS) is an intelligent data-driven method that can obtain satisfactory SOC estimation solutions against changing environmental conditions, but it has a complex structure and lengthy computation process [25].

1.2. Major Contributions

The main contribution of this research is to design an optimized data-driven algorithm-based SOC estimation technique for lithium-ion batteries. In particular, a time-delay neural network (TDNN) algorithm optimized by the improved firefly algorithm (iFA) is proposed to elevate the accuracy and robustness in SOC evaluation. The significant contributions of this research work are explained below:

- The data pre-processing of the proposed iFA-based TDNN algorithm is simple and has easy execution which only requires sensors to monitor the battery variables including voltage, current, and temperature, thereby avoiding the need for an added filter.
- The TDNN has a self-learning algorithm that updates the learning parameters and employs input layer information in the previous time steps to estimate SOC in the future stage. In contrast, the model-based SOC estimation techniques require depth information and knowledge about battery internal characteristics as well as experience and time to develop a battery model and estimate related parameters accurately.
- The traditional TDNN algorithm examines SOC with a trial and error approach to determine the suitable values of input time delay (UTD) and hidden neurons (HNs) [26]. However, the trial and error method has some drawbacks such as inefficiency, data under-fitted, and over-fitted issues. Therefore, the TDNN algorithm is integrated with iFA to avoid the trial and error method and achieve accurate SOC estimation solutions.
- The generalization capability of the iFA-based TDNN algorithm is tested with two dissimilar types of lithium-ion batteries. Moreover, two suitable experimental tests are carried out to validate the proposed algorithm.
- Apart from the experiments, the accuracy of the proposed method is examined using three EV drive cycles such as the dynamic stress test (DST), federal urban drive schedule (FUDS), and US06. Accordingly, the variation of SOC estimation is monitored at three different temperature conditions.
- The influence of electromagnetic interference and low sensor precision might lead to inaccuracy in measured current and voltage values. Thus, this paper considers uncertainty issues such as noise impacts and aging profiles while estimating SOC. The robustness and effectiveness of the iFA-based TDNN method are verified against both bias noise and random noise. The performance of lithium-ion batteries deteriorates after the battery is repeatedly charged and discharged a hundred times. Therefore, the adaptability of the proposed method is assessed under 50, 100, 150, and 200 aging cycles.

The remainder of the paper is organized into six sections. Section two covers the explanation of the proposed algorithm framework. The lithium-ion battery test bench and related experimental tests are outlined in section three. Section four illustrates the design, methodological structure and the execution of the proposed algorithm. The SOC estimation results under various conditions are delivered in section five. The conclusion is presented in section six.

2. Theoretical Framework of SOC Algorithm

This section explains the theoretical strategy and framework of the proposed optimized data-driven algorithm for SOC estimation in lithium-ion batteries.

2.1. SOC Modeling with Time Delay Network Algorithm

TDNN is a modified version of the feedforward neural network (FNN) which is simple, fast, and efficient. TDNN is a supervised machine learning algorithm that is well-suited to model a dynamic system with large time delays. Generally, FNN has no internal memory for storing past information, which is ineffective for solving time-series problems. TDNN overcomes this issue by having a past memory with tapped delay lines. TDNN exhibits dynamic memory and employs multiple layers under a necessary interconnection between units which confirms the capability to address non-linear and complex decisions [27]. TDNN has intelligent self-learning skills and robust computation abilities, and hence it is suitable for SOC estimation.

The structure of TDNN is designed using one input layer, one or more hidden layers, and one output layer, as shown in Figure 1. This research uses one hidden layer to estimate SOC. TDNN employs a series of data such as an input vector with UTD ($x = x_k, x_{k-1}, \dots, x_{k-i+1}$), HNs ($h = h_1, \dots, h_L$),

and output vector y_k to examine SOC. The output of the network can be expressed mathematically using the following equations:

$$y_k = \varphi_0 \left(\sum_{j=1}^L w_{oj} \cdot \varphi_j \left(\sum_{i=1}^M x_{k-i+1} w_{ji} + b_j \right) + b_o \right) \tag{1}$$

where φ_j and φ_0 denote the output of the hidden layer and output layer, respectively; w_{ji} is the weight between the input layer and hidden layers, w_{oj} is the weight between the hidden layer and output layer; b_j and b_o denote the hidden layer bias and output layer bias, respectively; M and L represent the number of inputs and hidden neurons, respectively.

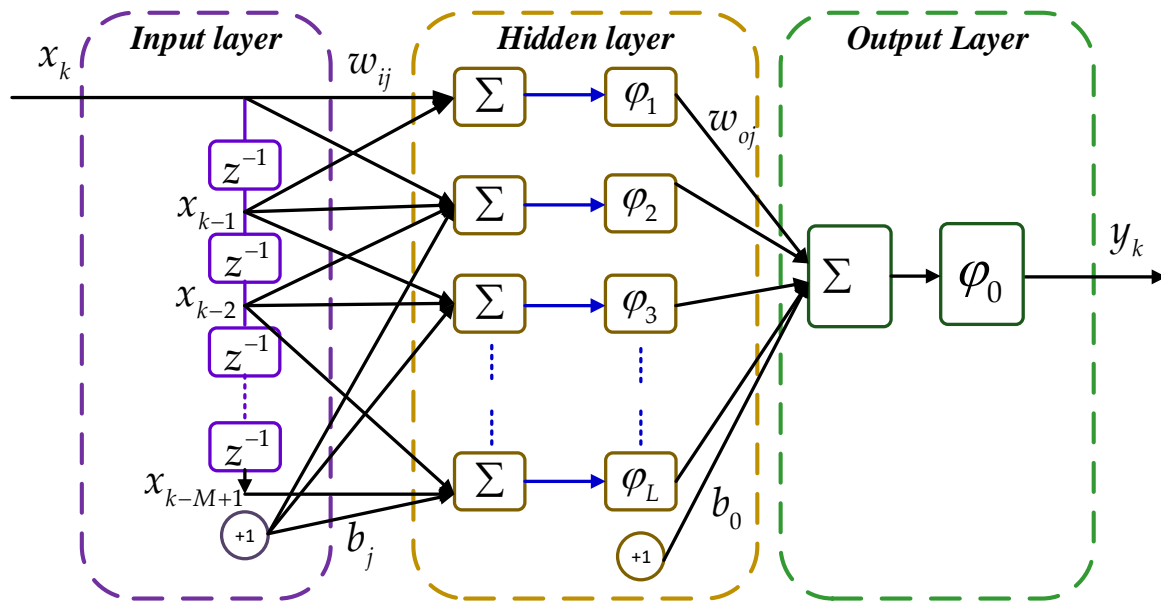


Figure 1. The time-delay neural network (TDNN) configuration for state-of-charge (SOC) estimation of the lithium-ion battery.

The sigmoid activation function is represented by $\varphi(t)$ and it is expressed as,

$$\varphi(t) = \frac{1}{1 + e^{-t}} \tag{2}$$

The back-propagation learning algorithm is applied to update network parameters of the TDNN algorithm including weights and bias by propagating the output error from the output layer to the hidden layer [28]. The Levenberg–Marquardt (LM) optimization technique is employed to train the TDNN due to its high accuracy and fast response toward the training operation [29]. LM updates the parameters adaptively to minimize the sum of the squared error, as shown in the following equations:

$$E(w) = \bar{e}(w)^T \bar{e}(w) = \sum_{k=0}^{\infty} \|e_k(w)\|^2 \tag{3}$$

where $\bar{e}(w)$ is the vector with element $e_k(w)$; $e_k(w)$ denotes the error in the k -th epoch.

A first-order Taylor series is employed to expand the error vector if the difference between the past weight vector and newly estimated weight vector becomes small [30]. The Newton method is used to reduce the function $E(w)$ with respect to w , as presented in the following equation.

$$\Delta w = -[\nabla^2 E(w)]^{-1} \nabla E(w) \tag{4}$$

where $\nabla E(w)$ stands for gradient and $\nabla^2 E(w)$ denotes the Hessian matrix which can be obtained using the following equation:

$$\nabla E(w) = J^T(w)\bar{e}(w) \quad (5)$$

$$\nabla^2 E(w) = J^T(w)J(w) + \sum_{k=1}^N e_k(w) \frac{\partial^2 e_k(w)}{\partial w_i \partial w_j} \quad (6)$$

where $J(w)$ denotes the Jacobian matrix which includes the first derivative of the network error. Since the second term of Equation (6) is trivial in comparison to the product of the Jacobian matrix, then Equation (4) can re-written as,

$$\Delta w = -[J^T(w)J(w)]^{-1} J^T(w)\bar{e}(w) \quad (7)$$

If the simplified Hessian matrix is found not invertible, then LM algorithm is adjusted and accordingly, Gauss-Newton method becomes,

$$\Delta w = -[J^T(w)J(w) + \gamma I]^{-1} J^T(w)\bar{e}(w) \quad (8)$$

where γ is the parameter to confirm the term $[J^T(w)J(w) + \gamma I]$ is positive and invertible, I is the identity matrix. The selection of the appropriate value of γ is essential for the LM function to ensure the steadiness and convergence speed.

2.2. Improved Firefly Algorithm

The concept of the FA is derived based upon the flashing characteristics of fireflies. The fireflies use different flashes to communicate among themselves as well as attract potential prey and mating partners [31]. Three statements are applied to develop FA. The first statement mentions that the attraction between two fireflies is independent since all the fireflies are unisex. The second statement declares that the brighter fireflies attract the less-bright fireflies. The fireflies with the same brightness travel randomly inside the boundary. The third statement says that the brightness of the fireflies will define the fitness function [32].

The standard FA has slow convergence issues when the fireflies are located far away in the early phases of generation. Moreover, the technique used to find the potential prey or communicate with mating partners in standard FA is mimicked. Also, the influence of environmental factors on the visibility of the flashing light is ignored. Generally, the attractiveness/ brightness of FA relies on many factors, such as the type and shape of the landscape, the distance between two fireflies, and a few environmental factors. For instance, the brightness visibility is reduced in the presence of fog, while the attractiveness/brightness rises as darkness increases. Likewise, the brightness of fireflies cannot be seen in the presence of high-intensity light. To address these concerns, Ball et al. [33] proposed a new improved FA (iFA) algorithm (Algorithm 1) to increase the convergence speed by updating the brightness of the fireflies. The exploration and exploitation capacities are enhanced in iFA algorithm by adding two new terms: brightness visibility (L_{mod}) and environmental factors (ξ).

Generally, the probability of brightness visibility increases in the lower-dimension landscape and easy optimization problems. In that case, L_{mod} is assigned to a high value. In contrast, L_{mod} is set to lower value when the brightness visibility decreases in the high dimensional and complex optimization problems. The impacts of environmental factors also affect the brightness visibility of iFA. Thus, two environmental variables are introduced, including ambient darkness (σ_1) and ambient foginess (σ_2). The connection between these two variables can be expressed as follows:

$$\zeta = \frac{1}{1 + e^{-\left(\frac{\sigma_2}{\sigma_1 \ln(i_{gen})}\right)}} \tag{9}$$

where i_{gen} denotes the generation number varying between 0 and i_{MaxGen} . The brightness of fireflies can be written as follows:

$$\beta(r) = \beta_0^{Proposed} e^{-\gamma r^m}, (m \geq 1) \tag{10}$$

where the attractiveness for $r = 0$ is represented by β_0 ; γ is the absorption coefficient of light, r is the distance between fireflies. The distance between two fireflies, r_{ij} is based on the cartesian coordinate system that can be written as follows:

$$r_{ij} = \|x_i - x_j\| = \sqrt{\sum_{k=1}^d (x_{i,k} - x_{j,k})^2} \tag{11}$$

where $x_{i,k}$ and $x_{j,k}$ are the spatial coordinate of the i -th and j -th fireflies towards the k -th component.

The proposed attractiveness of fireflies ($\beta_0^{Proposed}$) is defined in the following equations:

$$\beta_0^{Proposed} = (\beta_0 \times L_{mod}) + \zeta \text{ when } rand \leq \zeta_{seed} \tag{12}$$

$$\beta_0^{Proposed} = \beta_0 \text{ when } rand > \zeta_{seed} \tag{13}$$

If the ambient darkness increases, the contributions from the second term of Equation (12) will be reduced, resulting in a lower environmental effect on $\beta_0^{Proposed}$. In opposition, if the intensity of ambient darkness decreases, then the impact of the environment becomes stronger, yielding lower brightness visibility of fireflies. The rise of ambient fogginess in the environment leads to a stronger impact of the environmental factor (ζ) on the proposed brightness of fireflies ($\beta_0^{Proposed}$).

During the early iteration of iFA, the fireflies are located far away from one another, and accordingly, the effect on environmental factors becomes stronger. As the iteration starts to increase, the fireflies are situated close to each other, and subsequently their brightness visibility increases. In this case, the environmental factor has less impact on the brightness visibility of iFA. Therefore, a probability index (ζ_{seed}) is formulated using i_{gen} and normalized between 0 and 1.

$$\zeta_{seed} = 1 - \frac{i_{gen}}{i_{MaxGen}}; 1 \leq i_{gen} \leq i_{MaxGen} \tag{14}$$

If the random number $rand$ is equal to or lower than ζ_{seed} , then Equation (12) will be executed; otherwise, Equation (13) will be selected. The brighter firefly j is attracted by the lesser bright firefly i , as expressed by,

$$x_{i_new} = x_{i_old} + \beta_0^{Proposed} e^{-\gamma r_{ij}^m} (x_j - x_{i_old}) + \alpha \epsilon_i \tag{15}$$

where α is the randomization parameter and ϵ_i defines the random numbers located between '0' and '1'.

The pseudocode of iFA is illustrated below:

Algorithm 1 Improved Firefly Algorithm (iFA)**Start**

Define the fitness function $f(x)$, $x = (x_1, \dots, x_d)^T$

Create initial population of fireflies $i = 1, 2, \dots, Size_{population}$

Assign γ α β_0 L_{mod} σ_1 and σ_2

Assess fitness function of individual fireflies $f(x), i = 1, 2, \dots, Size_{population}$

While $t < Max_{generation}$

Assess ξ_{seed} with Equation (14)

if $\xi_{seed} \geq rand$

Assess $\beta_0^{Proposed}$ with Equation (12)

else

Assess $\beta_0^{Proposed}$ with Equation (13)

end if

for $i = 1 : Size_{population}$

for $j = 1 : Size_{population}$

if $f(x_j) > f(x_i)$

Move firefly i toward j

End if

Update the attractiveness of fireflies (β) with Equation (10)

Assess new solutions and update light intensity with Equation (15)

end for j

end for i

Rank the fireflies and find the current best population

$t = t + 1$

end while

3. Lithium-Ion Battery Experiments and Data Preparation

This section covers the type of lithium-ion cells used in this research, collected dataset, experimental arrangement, experimental procedures, data partition, and evaluation criteria.

3.1. Lithium-Ion Battery Cell

In this research, two popular EV lithium-ion battery cells are used; one is a 3200 mAh rated NCR18650B manufactured by Panasonic and the other is a 2600 mAh rated ICR18650-26F developed by Samsung. The positive electrodes of NCR18650B and ICR18650-26F are made using LiNiCoAlO₂ (LiNCA) and LiNiMnCoO₂ (LiNMC), respectively, while the graphite is used as a negative electrode in both batteries. LiNMC is popular due to its extended lifespan, while LiNCA offers a high level of specific energy. Table 1 provides the information and specifications of the two lithium-ion batteries [6].

Table 1. Specifications of the lithium-ion battery.

Parameters	LiNiCoAlO ₂	LiNiMnCoO ₂
Nominal capacity (Ah)	3.2 Ah	2.6 Ah
Nominal Voltage (V)	3.6	3.7
Min/Max voltage (V)	2.5/4.2	2.75/4.2
Charging method	CC-CV	CC-CV
Charging time (hours)	4	3
Charging current (mA)	1625	1300
Specific Energy (Wh/kg)	200–260	150–220
Weight (g)	48.5	47.0
Lifespan (cycles)	500	1000–2000
Thermal runaway (temperature)	150 °C	210 °C

3.2. Battery Experimental Setup

A lithium-ion battery test bench model is established to monitor the key parameters including capacity, current and voltage, power, and cycle number. The developed test bench model is separated into two sections: one is the hardware section and the other is the software section, as depicted in Figure 2. The hardware section includes two segments; the measurement unit and the control unit. The measurement unit is designed using NEWARE BTS-4000 and LiNCA, LiNMC battery cells. The maximum capacity of voltage and current for NEWARE BTS-4000 are 5 V and 6 A, respectively. The NEWARE BTS-4000 has 8 channels that are independent of each other and it is capable of sensing and recording the battery parameters each second with an accuracy of $\pm 0.05\%$ full scale (FS) [34]. The control unit can keep the charging and discharging voltage under the defined cut-off values, thus protecting the battery from overcharging and over-discharging issues. In contrast, the software section includes the battery testing system (BTS) software version 7.6 related to NEWARE BTS-4000 hardware and MATLAB 2015a. Both pieces of software are installed on the host computer. Each step of the SDT and HPPC experiment is executed through the BTS software. After, the recorded data are transferred to the host computer. Besides, the charging and discharging control of LiNCA and LiNMC batteries are implemented through the appropriate software function of the BTS software. Finally, MATLAB 2015a software is used to execute the iFA-based TDNN algorithm code to examine SOC.

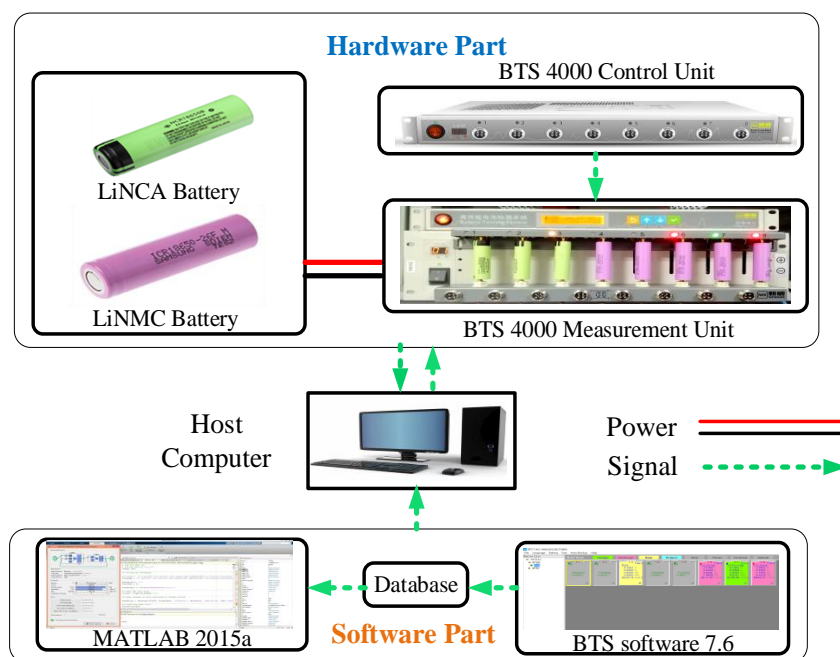


Figure 2. The lithium-ion battery test bench model configuration for SOC estimation.

3.3. Battery Experimental Tests

The validation of the proposed algorithm is performed using a static discharge test (SDT) and a hybrid pulse power characterization (HPPC) test. Besides, the noise test and aging cycle tests are carried out to check the SOC accuracy against uncertainties. Before the experiments begin, the battery is completely charged, and accordingly, the initial SOC is assigned to 100%. The Samsung ICR18650-26F battery is used to explain the steps of each experimental test. These steps can also be applied to a Panasonic NCR18650B while maintaining the manufacturer's requirements in terms of current and voltage.

- (1) SDT SDT uses the constant discharge current of the lithium-ion battery to evaluate SOC. The operation of SDT is explained using the steps mentioned below.

- i. Firstly, a constant current (CC) of 1.3 A (0.5 C) is applied to charge the battery fully until the charge voltage increases to the maximum threshold of 4.2 V.
 - ii. Then, a constant voltage (CV) of 4.2 V is applied until a drop in the charge current to 0.13 A (0.05 C) is achieved.
 - iii. The battery being tested is kept idle for 1 h.
 - iv. A discharge current of 2.6 A (1 C) is applied until the voltage is reduced to 2.75 V.
 - v. The test ends if the battery voltage reaches the minimum threshold of 2.75 V; otherwise, step ii will continue.
- (2) HPPC test The HPPC test consists of the array of charge and discharge current pulses arranged in an orderly manner. The following steps are used to describe the operation of HPPC.
- i. The CC-CV method is employed to charge the battery completely until the battery current decreases to 0.13 A (0.05 C).
 - ii. The battery being tested is kept idle for 1 h.
 - iii. A discharge current of 1.3 A (0.5 C) is applied for 10 s.
 - iv. The battery being tested is kept idle for 3 min.
 - v. A charge current of 1.3 A (0.5 C) is applied for 10 s.
 - vi. The battery is kept idle for 3 min.
 - vii. A discharge current of 0.65 A (0.25 C) is applied for 24 min to decrease the SOC capacity of the battery by 10%.
 - viii. The experiment ends if the battery voltage reaches the lower cut off voltage; otherwise, step iii will start again.

(3) Noise test

The accuracy of SOC could deviate due to electromagnetic interference (EMI) noises and sensor precision. EMI noises take place when the switching of the power converter is operated at a high frequency, and hence they may combine with the measured current and voltage signals. On the other hand, current and voltage sensors have a common issue, equipment error, which leads to errors in measurements. Thus, this research work considers both EMI impacts and sensor precision by adding random noises and bias noises, respectively, to evaluate the proposed model's suitability in the real-world environment. Accordingly, the positive bias noises of 0.1 A and 0.01 V are injected into the current and voltage measurements, respectively. At the same time, the random noises having amplitude values of 0.1 A and 0.01 V are included in current and voltage measurements, respectively.

(4) Aging cycle test

Battery aging is a significant index term used to evaluate performance after continuous charge-discharge cycles. Usually, the capacity of the battery declines with the rise of aging cycles. However, capacity degradation does not occur in the same way in different types of lithium-ion batteries. In this research, LiNCA and LiNMC battery cells are employed to assess the aging effect on performance and predictable capacity, as well as to evaluate SOC. Four milestones of aging cycles are selected to validate the accuracy and robustness of the proposed method including 50, 100, 150, and 200 cycles. The steps of the aging cycle are highlighted as follows:

- i. Firstly, the complete charge operation is executed based on the CC-CV method with a constant charge current of 1.3 A (0.5 C) until the battery voltage reaches 4.2 V. After, the charge voltage of 4.2 V is kept constant until the charging current declines to 0.13 A (0.05 C).
- ii. The idle operation of the battery is performed for 15 min.
- iii. A constant discharge current of 2.6 A (1 C) is applied until the battery voltage decreases to 2.75 V.

- iv. The lowest point of the discharge voltage (2.75 V) of the battery is checked. The one aging schedule is completed when the battery reaches a cut-off voltage of 2.75 V; otherwise, step iii will begin again.
- v. After the completion of one aging cycle, the battery is kept in an idle operation stage for one hour.
- vi. Step i starts again to perform the second aging cycle test. The process continues until the defined cycles are achieved.

3.4. Dataset Training and Testing

The dataset achieved from the battery test bench is split into two groups; training and testing. The data partition is performed based on the cross-validation method using a 70-30 ratio [35]. The training operation is implemented in the offline phase while testing operation and SOC estimation is performed in the online phase. To improve training accuracy and speed, the dataset is normalized within the boundary of $[-1, 1]$, as represented by the equation below,

$$x' = \frac{2(x - x_{\min})}{x_{\max} - x_{\min}} - 1 \tag{16}$$

where x_{\max} and x_{\min} are the maximum and the minimum values of variable x , respectively. The maximum iterations and performance goal are set to be 1000 and 0.000001, respectively. The learning rate is considered as 0.5. The host computer has sufficient computational power with 12 GB random access memory (RAM). The current and voltage load profiles of SDT and HPPC for the LiNCA and LiNMC batteries are shown in Figures 3 and 4, respectively. In this research, the positive current and negative current correspond to the charging process and the discharging process, respectively. The relationship between SOC and voltage is established where voltage increases with the rise of SOC, as illustrated in Figure 5.

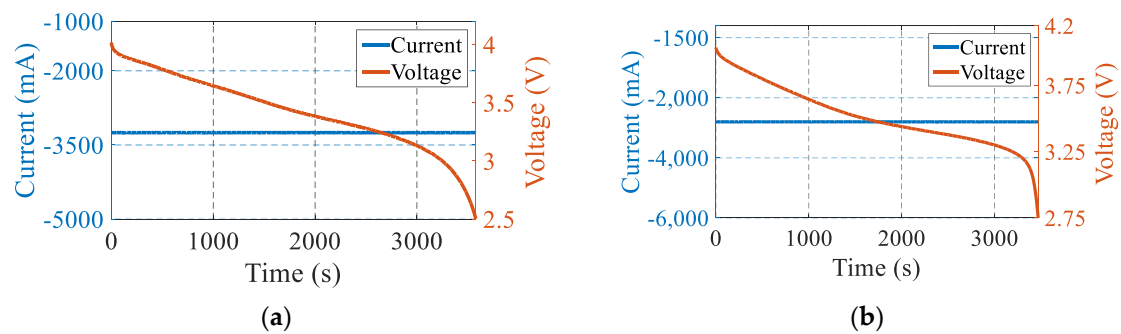


Figure 3. SDT load profile of (a) the LiNCA battery and (b) the LiNMC battery.

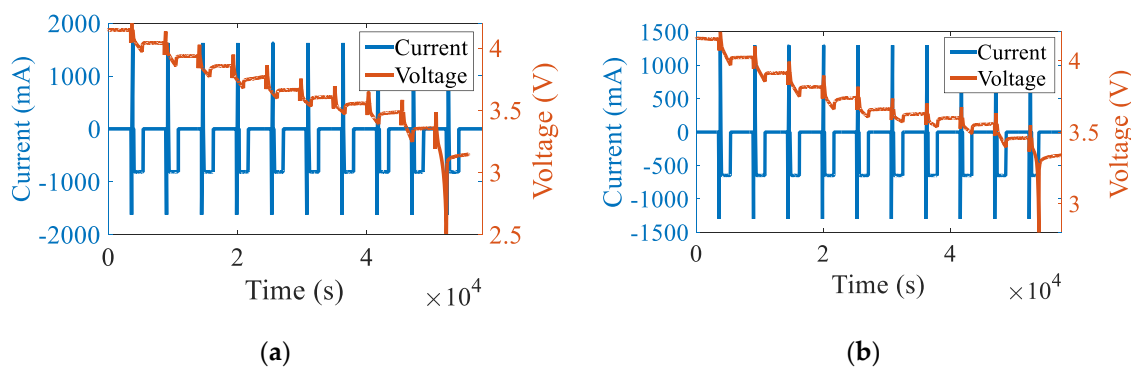


Figure 4. HPPC load profiles of (a) the LiNCA battery and (b) the LiNMC battery.

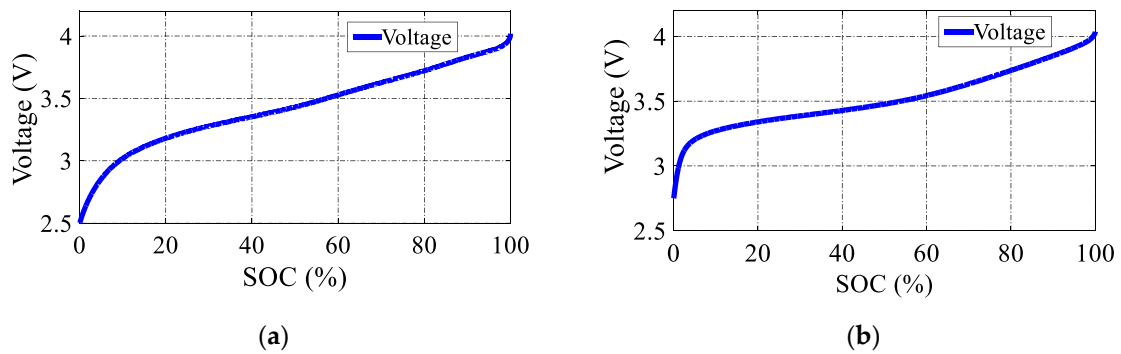


Figure 5. The relationship between SOC and voltage for (a) the LiNCA battery and (b) the LiNMC battery.

3.5. Measurement of SOC Effectiveness

The performance of the iFA-based TDNN algorithm is assessed by comparison with reference SOC values achieved through the CC method with an adjustable current sensor. The different statistical error rate terms shown in (17)–(22) are used to check the accuracy of the proposed algorithm [35].

$$SOC\ error = SOC_{a_i} - SOC_{es_i} \tag{17}$$

$$RMSE = \sqrt{\frac{1}{N} \sum_{i=1}^N (SOC_{a_i} - SOC_{es_i})^2} \tag{18}$$

$$MSE = \frac{1}{N} \sum_{i=1}^N (SOC_{a_i} - SOC_{es_i})^2 \tag{19}$$

$$MAE = \frac{1}{N} \sum_{i=1}^N (SOC_{a_i} - SOC_{es_i}) \tag{20}$$

$$MAPE = \frac{1}{N} \sum_{i=1}^N \left| \frac{SOC_{a_i} - SOC_{es_i}}{SOC_{a_i}} \right| \tag{21}$$

$$SD = \sqrt{\frac{1}{N-1} \sum_{i=1}^N (SOC\ error - \overline{SOC\ error})^2} \tag{22}$$

where SOC_a is the actual/reference SOC and SOC_{es} is the estimated SOC by the proposed algorithm, N is the number of the data sample, MSE is mean square error, MAE is mean absolute error, MAPE is mean absolute percentage error, SD is the standard deviation, and $\overline{SOC_{error}}$ is the average error of SOC estimated values.

4. Design and Implementation of iFA Based TDNN Algorithm for SOC Estimation

The proposed algorithm is designed based on three vital components, including input dimension, fitness function, and constraints of optimization. The iFA determines the suitable values of the hyper-parameters which include the UTD and HNs while achieving the minimum value of the fitness function and satisfying all constraints in the optimization during the iterative method.

4.1. Input Information

The input information consists of a matrix that is designed using the number of rows and columns and defines the dimension and boundary of the hyperparameters. The number of problem dimension is characterized by the number of rows, while the population of hyperparameters is outlined by the number of columns in the matrix, as represented by the equation below:

$$D_{ij} = \begin{bmatrix} X_{11} & X_{12} & X_{13} & \dots & X_{1j} \\ X_{21} & X_{22} & X_{23} & \dots & X_{2j} \\ X_{31} & X_{32} & X_{33} & \dots & X_{3j} \\ \\ X_{41} & X_{42} & X_{43} & \dots & X_{4j} \\ \vdots & \vdots & \vdots & \dots & \vdots \\ X_{i1} & X_{i2} & X_{i3} & \dots & X_{ij} \end{bmatrix} \quad (23)$$

where D_{ij} represents the matrix of the input data which can be defined by i and j , where $i = 1, 2, \dots, P$, with P representing the population number; $j = 1, 2, \dots, N$, with N denoting the problem dimension.

4.2. Fitness Function

The fitness function helps to achieve precise SOC estimation outcomes by finding the appropriate values of hyperparameters. The iFA aims to obtain the lowest error rate of fitness function through iterations that correspond to the optimum values of the UTD and HNs. Lithium-ion battery SOC estimation has a high volume of datasets where SOC error is distributed randomly. Thus, root means square error (RMSE) is selected as the fitness function which is shown in the following equation:

$$\text{Objective function} = \min (\text{RMSE}) \quad (24)$$

4.3. Optimization Constraints

The optimization constraints are determined by assigning the upper and lower number of the UTD and HNs of the

TDNN algorithm. If the population of hyperparameters is located outside the boundary, then the accuracy of iFA could deviate which may result in unsatisfactory performance during SOC estimation. Therefore, the values of hyperparameters are checked in each iteration. If any values are located outside the boundary, then values will be reproduced and updated accordingly. The constraints of the hyperparameters must satisfy the following equation:

$$X_{i,j}^{k-1} < X_{i,j}^k < X_{i,j}^{k+1} \quad (25)$$

The above equation indicates that the value $X_{i,j}^k$ of the hyperparameter should be placed between $X_{i,j}^{k-1}$ and $X_{i,j}^{k+1}$.

4.4. Execution Process of iFA Based TDNN Algorithm

The implementation of the TDNN-iFA begins with the collection of battery datasets, including current and voltage, through experimental tests. After that, iFA is employed to find the appropriate value of UTD and HNs based on the lowest value of the fitness function. Finally, the accuracy and robustness of SOC estimation are assessed using different performance indicator terms. The proposed method is then advanced into different tests and uncertainties. The flow diagram of the proposed algorithm is shown in Figure 6. The methodology of the TDNN-iFA algorithm is divided into three stages.

In stage I, a battery test bench model is built to carry out the experiments as well as collect battery data. Then, data is pre-processed through normalization. After, the data is separated into training and testing groups.

In stage II, the implementation of TDNN starts with assigning the epoch number, performance goal, and learning rate. Subsequently, the process of iFA starts with the selection of suitable iteration number, population size, input dimension, fitness function, and optimization constraints. At first, the initial population of iFA is generated and the fitness function is assessed. After, the light intensity of

the firefly is evaluated based on the fitness function, and accordingly, the best population is determined. Later, the probability index and proposed attractiveness are assessed using Equations (12) and (13). Next, the movement of the firefly from the brighter one toward the less-bright one is estimated. Later, attractiveness among fireflies is evaluated and light intensity is updated using Equations (10) and (15), respectively. The aforementioned processes continue until the highest number of iterations is completed. Finally, the optimal values of UTD and HNs are found and consequently proceed to the TDNN algorithm. Accordingly, the TDNN training process is executed using the LM method using Equations (3)–(8). Afterward, the network parameters of TDNN are updated using the backpropagation learning rule. Finally, the output of TDNN is computed using Equation (1).

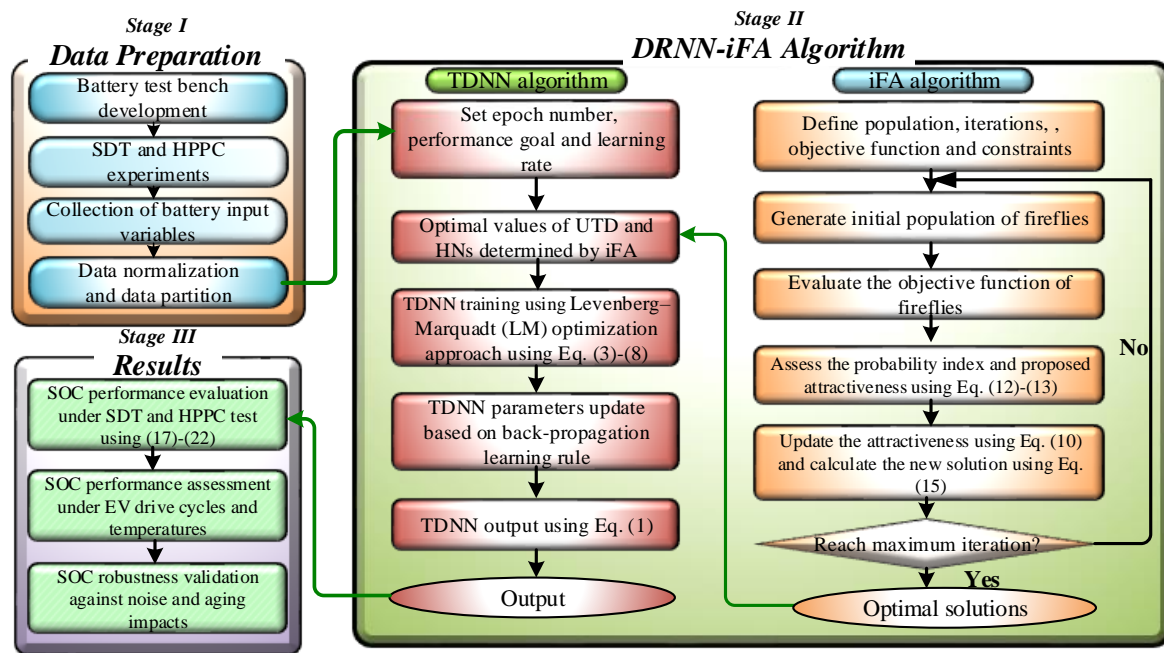


Figure 6. The methodological framework of the iFA-based TDNN algorithm for SOC estimation.

In stage III, the TDNN-iFA algorithm is verified through SDT and HPPC experiments based on statistical error rate terms, as indicated in Equations (17)–(22). In line with that, the effectiveness of the TDNN-iFA algorithm is assessed under EV drive cycles and varying temperature situations. Besides, the robustness of the proposed method is evaluated against the uncertainties, including noise tests and the aging cycle tests.

5. SOC Experimental Results and Validation

This section describes the experimental results of SOC estimation under different chemistries of lithium-ion battery cells. Also, the validation of SOC is carried out under EV drive cycles, noise effects, and aging impacts.

5.1. Assessment of Fitness Function and Optimal Parameter

The fitness function is evaluated using the optimization response curve in SDT and HPPC experiments for LiNCA and LiNMC batteries, as presented in Figures 7 and 8, respectively. The fitness function performance of iFA is compared with FA and particle swarm optimization (PSO). The optimization curve is generated using a population of 50 and 500 iterations.

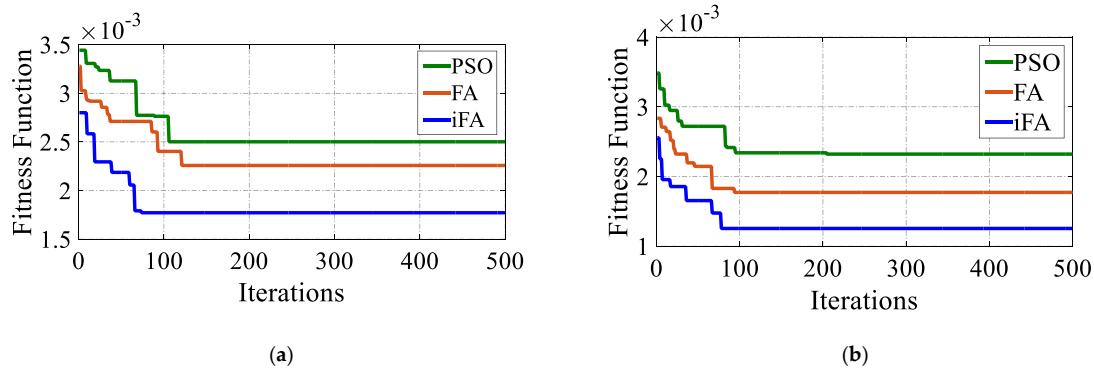


Figure 7. The response curve for optimization in the SDT load profile of (a) the LiNCA battery and (b) the LiNMC battery.

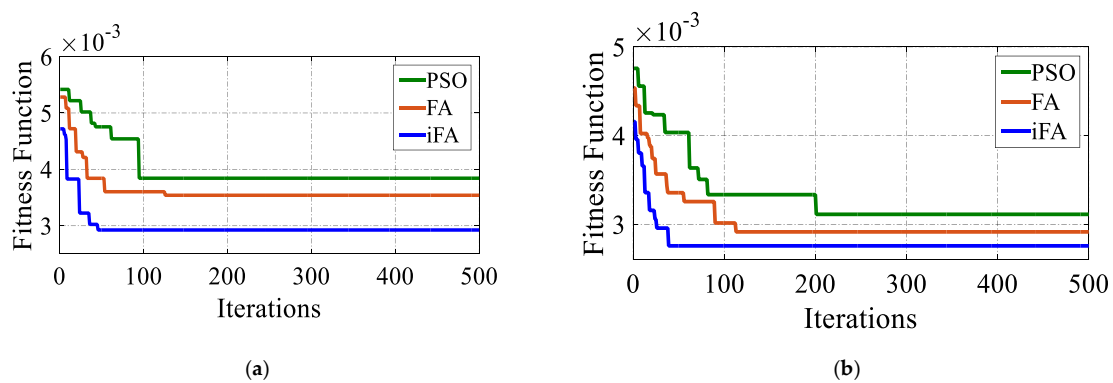


Figure 8. The response curve for optimization in the HPPC load profile of (a) the LiNCA battery and (b) the LiNMC battery.

The optimal values of UTD and HNs are determined via the response curve for optimization by identifying the lowest point of the fitness function. For example, in SDT, iFA achieves the lowest fitness function after 74 and 78 iterations for the LiNCA and LiNMC battery, respectively, which are smaller than the FA and PSO algorithms. The corresponding iteration number delivers the fitness functions of 0.177% and 0.125% and provides the best values of the UTD and HNs of 2, 3, and 12, 15, respectively. Likewise, in the HPPC test, iFA demonstrates excellent solutions in obtaining the minimum value of the fitness function compared to FA and PSO algorithms achieving 0.292% and 0.276% after 45 and 39 iterations, respectively, for the LiNCA battery and LiNMC battery. Accordingly, the optimal values of UTD and HNs of 4, 5, and 10, 18 are obtained after 45 and 39 iterations, respectively. The appropriate values of the UTD and HNs in SDT and HPPC tests are summarized in Table 2.

Table 2. Optimum hyperparameters of the TDNN-iFA algorithm in SDT and HPPC tests.

Battery Test	Optimal Hyperparameters	LiNCA Battery	LiNMC Battery
SDT	UTD	2	3
	HNs	12	15
HPPC	UTD	4	5
	HNs	10	18

5.2. Experimental Verification Results

The performance of the iFA-based TDNN algorithm is verified using SDT and HPPC experiments and results are compared and analyzed with three commonly-reported data-driven algorithms; namely, the backpropagation neural network (BPNN) and radial basis function neural network (RBFNN) and Elman neural network (ENN). The comparative analysis is performed using a similar length of input

datasets for training and testing. In addition, iFA is employed to update the number of HNs of BPNN, RBFNN, and ENN to achieve unbiased comparison.

(1) SOC Estimation in LiNCA Battery

The SOC is examined for the LiNCA battery using the TDNN-iFA algorithm under SDT and HPPC experiments, as depicted in Figures 9 and 10, respectively. It is observed that the reference SOC values are placed adjacent to estimated SOC values which proves that the proposed approach obtains accurate solutions. The results of RMSE, MAE, MAPE, and SD also demonstrate the superiority of the iFA-based TDNN algorithm over iFA-based BPNN, iFA-based RBFNN, iFA-based ENN as denoted in Table 3. In SDT, RMSE is estimated to be 0.5844% in the proposed algorithm, which is a 32.2%, 54.9%, and 19% decrease when compared to the iFA-based BPNN, iFA-based RBFNN, iFA-based ENN, respectively. Moreover, the proposed algorithm computes MAE of 0.2374% which is reduced by 60.8%, 78.7% and 56.7% from those obtained from the iFA-based BPNN, iFA-based RBFNN, iFA-based ENN, respectively. Similarly, MAPE is declined by 29.9%, 54.1% and 38.7% in comparison to those values derived using the iFA-based BPNN, iFA-based RBFNN, iFA-based ENN. Besides, the proposed method has a maximum SOC error under 3%; however, high fluctuations are observed in iFA-based BPNN, iFA-based RBFNN, iFA-based ENN, having SOC error of [−5.19%, 6.45%], [−4.36%, 8.89%] and [−3.32%, 2.26%], respectively. The proposed algorithm is also dominant in HPPC test and possesses a lower error rate than those from iFA-based BPNN, iFA-based RBFNN, iFA-based ENN methods.

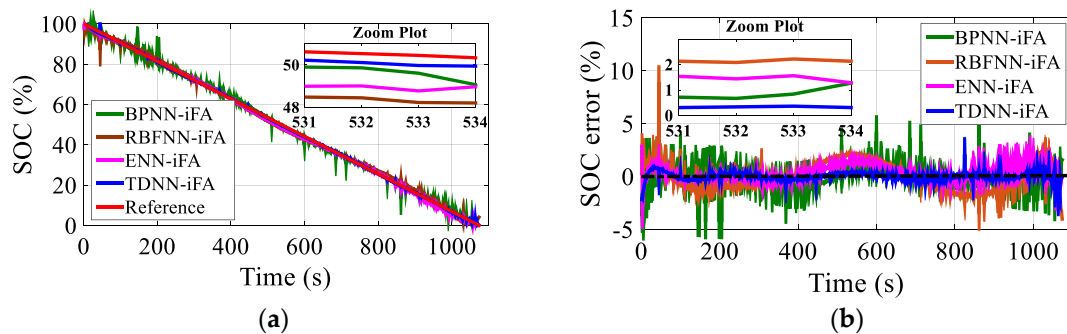


Figure 9. The experimental outcomes of SDT for LiNCA battery (a) SOC (b) SOC error.

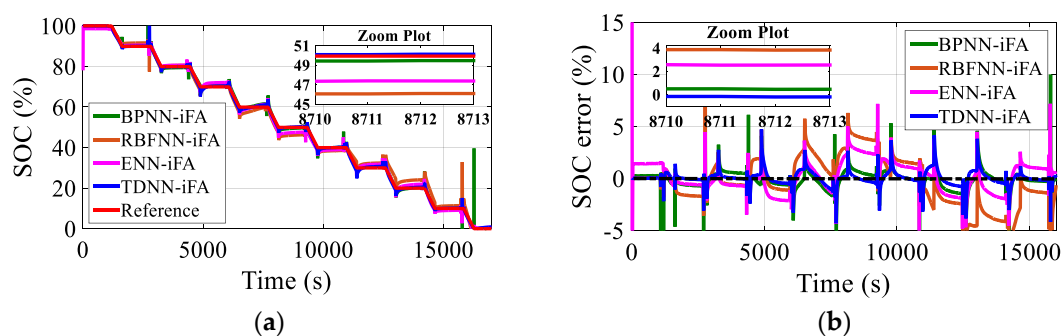


Figure 10. The experimental outcomes of HPPC for the LiNCA battery: (a) SOC, (b) SOC error.

Table 3. SOC performance evaluation in the LiNCA battery.

SOC Method	BPNN-iFA		RBFNN-iFA		ENN-iFA		TDNN-iFA	
Load Profile	SDT	HPPC	SDT	HPPC	SDT	HPPC	SDT	HPPC
RMSE (%)	0.8620	1.4124	1.2961	2.5155	0.7215	1.6524	0.5844	0.8512
MSE (%)	0.0074	0.0199	0.0168	0.0633	0.0052	0.0273	0.0034	0.0072
MAE (%)	0.6059	0.6659	1.1145	1.997	0.5479	1.2294	0.2374	0.4652
MAPE (%)	3.6939	6.2650	5.6405	10.4826	4.2235	7.5826	2.5864	3.5624
SD (%)	0.8610	1.1685	1.2815	2.4878	0.6876	1.4869	0.5841	0.8505
SOC error bound (%)	[−5.19, 6.45]	[−5.45, 9.98]	[−4.36, 8.89]	[−15.28, 12.32]	[−3.32, 2.26]	[−5.09, 7.17]	[−2.58, 2.05]	[−4.31, 4.73]

(2) SOC Estimation in LiNMC Battery

The performance of SOC estimation results is also evaluated for the LiNMC battery under SDT and HPPC experiments, as illustrated in Figures 11 and 12, respectively. From Table 4, it can be observed that RMSE is decreased by 60.3%, 70.8%, and 49.7% in the proposed algorithm under SDT compared to the iFA-based BPNN, iFA-based RBFNN, iFA-based ENN, respectively. Similarly, 76.2%, 84.3%, and 68.6% reductions are reported in the proposed algorithm in comparison to iFA-based BPNN, iFA-based RBFNN, and iFA-based ENN, respectively, while calculating MAE. Besides, the iFA-based TDNN method demonstrates excellent results in the aspects of SOC error, MSE and MAPE. For instance, the maximum SOC error is noted to be 1.38% in the proposed approach, while it is 3.31%, 5.44%, and 3.02% in iFA-based BPNN, iFA-based RBFNN, and iFA-based ENN, respectively. The proposed algorithm also obtains a narrow SOC error in the HPPC test, obtaining a maximum SOC error of 4.23%. Since TDNN has few mathematical complications in the testing stage, the execution time is small, indicating less than 30 milliseconds and 0.5 s in SDT and HPPC tests, respectively. In conclusion, the aforesaid accurate outcomes and fast computation time in the testing phase demonstrate the suitability of TDNN-iFA algorithms in real-time BMS.

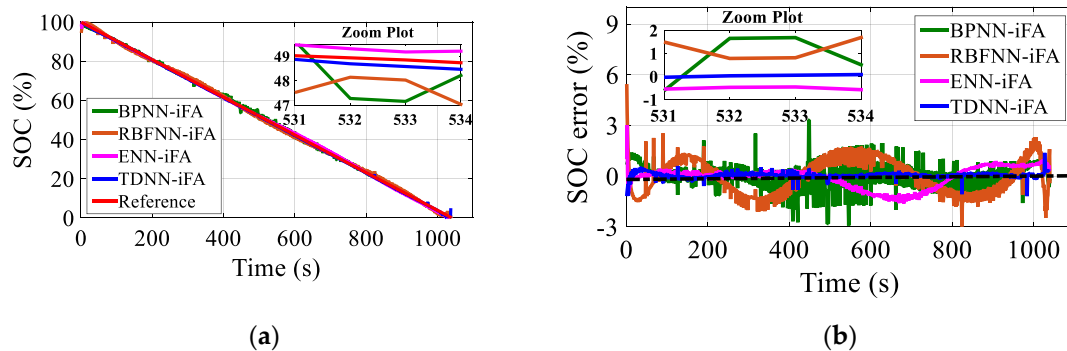


Figure 11. The experimental outcomes of SDT for LiNMC battery (a) SOC (b) SOC error.

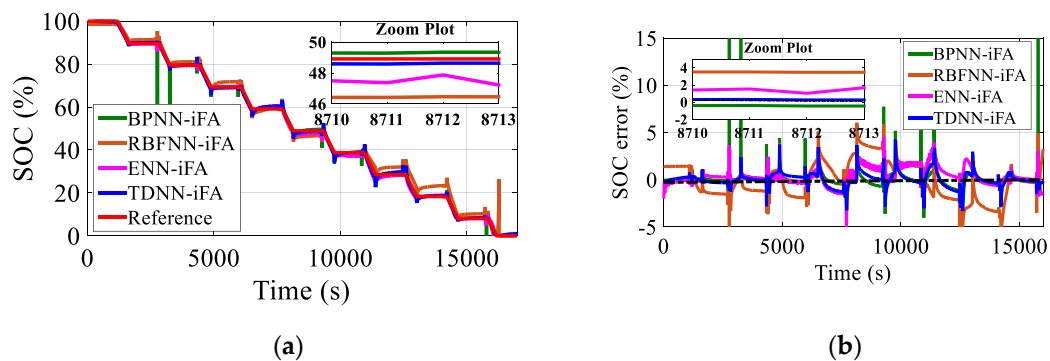


Figure 12. The experimental outcomes of HPPC for LiNMC battery (a) SOC (b) SOC error.

5.3. SOC Estimation under EV Drive Cycles and Temperatures

The accuracy and effectiveness of the iFA-based TDNN approach for SOC estimation are further evaluated under different EV drive cycles. EV drive cycle data are obtained on LiNMC battery with a rated capacity of 2.0 Ah [36]. The DST, FUDS, and US06 drive schedules are employed to assess the accuracy and robustness of the proposed method, as depicted in Figure 13. The aforementioned drive cycles are diverse in terms of current and voltage values. DST relates to the battery charging and discharging under the dynamic phase, FUDS relates to EV driving in urban areas and US06 corresponds to high acceleration driving with quick speed fluctuation. It is noticed that SOC estimation results under DST, FUDS, and US06 drive cycles are found to be located very near to the reference SOC values which confirms high robustness and low estimation error. In all drive cycles, SOC error is

restricted under $\pm 5\%$. Moreover, the temperature effects; $0\text{ }^{\circ}\text{C}$, $25\text{ }^{\circ}\text{C}$ and $45\text{ }^{\circ}\text{C}$ are taken into account under DST, FUDS, and US06 drive cycles, as shown in Figure 14. It is observed from Figure 13 that, iFA-based TDNN achieves RMSE and MAE below 0.8% and above 6% , respectively in DST drive cycle at $0\text{ }^{\circ}\text{C}$. The RMSE and MAE in the FUDS cycle are slightly higher than the DST cycle, indicating below 0.9% and 0.8% , respectively at $0\text{ }^{\circ}\text{C}$. US06 cycle obtains the highest error rates among all drive cycles due to high fluctuation of current values with RMSE and MAE below 1% and 0.8% respectively. It is observed that error rates in all drive cycles decrease with the rise of temperature from $0\text{ }^{\circ}\text{C}$ to $45\text{ }^{\circ}\text{C}$. For instance, RMSE in DST cycles is achieved to be over 0.6% at $25\text{ }^{\circ}\text{C}$ while it is below 0.6% at $45\text{ }^{\circ}\text{C}$. In the US06 cycle, iFA-based TDNN has MAE below 0.8% at $25\text{ }^{\circ}\text{C}$; however, MAE drops at $45\text{ }^{\circ}\text{C}$, indicating under 0.6% .

Table 4. SOC Performance Evaluation in LiNMC Battery.

SOC Method	BPNN-iFA		RBFNN-iFA		ENN-iFA		TDNN-iFA	
	SDT	HPPC	SDT	HPPC	SDT	HPPC	SDT	HPPC
RMSE (%)	0.7775	1.2989	1.0576	2.1121	0.6137	1.0272	0.3084	0.7937
MSE (%)	0.0065	0.0169	0.0112	0.0446	0.0038	0.0106	0.0009	0.0063
MAE (%)	0.6091	0.4222	0.9242	1.6669	0.4620	0.7265	0.1452	0.3283
MAPE (%)	3.7937	7.7595	7.1818	14.3527	4.2617	7.2337	2.1826	5.5247
SD (%)	0.7770	1.2982	1.0556	2.1115	0.6123	0.9818	0.3041	0.7940
SOC error bound (%)	[-2.94, 3.31]	[-5.47, 15.87]	[-2.97, 5.44]	[-10.87, 6.04]	[-1.62, 3.02]	[-5.24, 8.04]	[-1.18, 1.38]	[-3.32, 4.23]

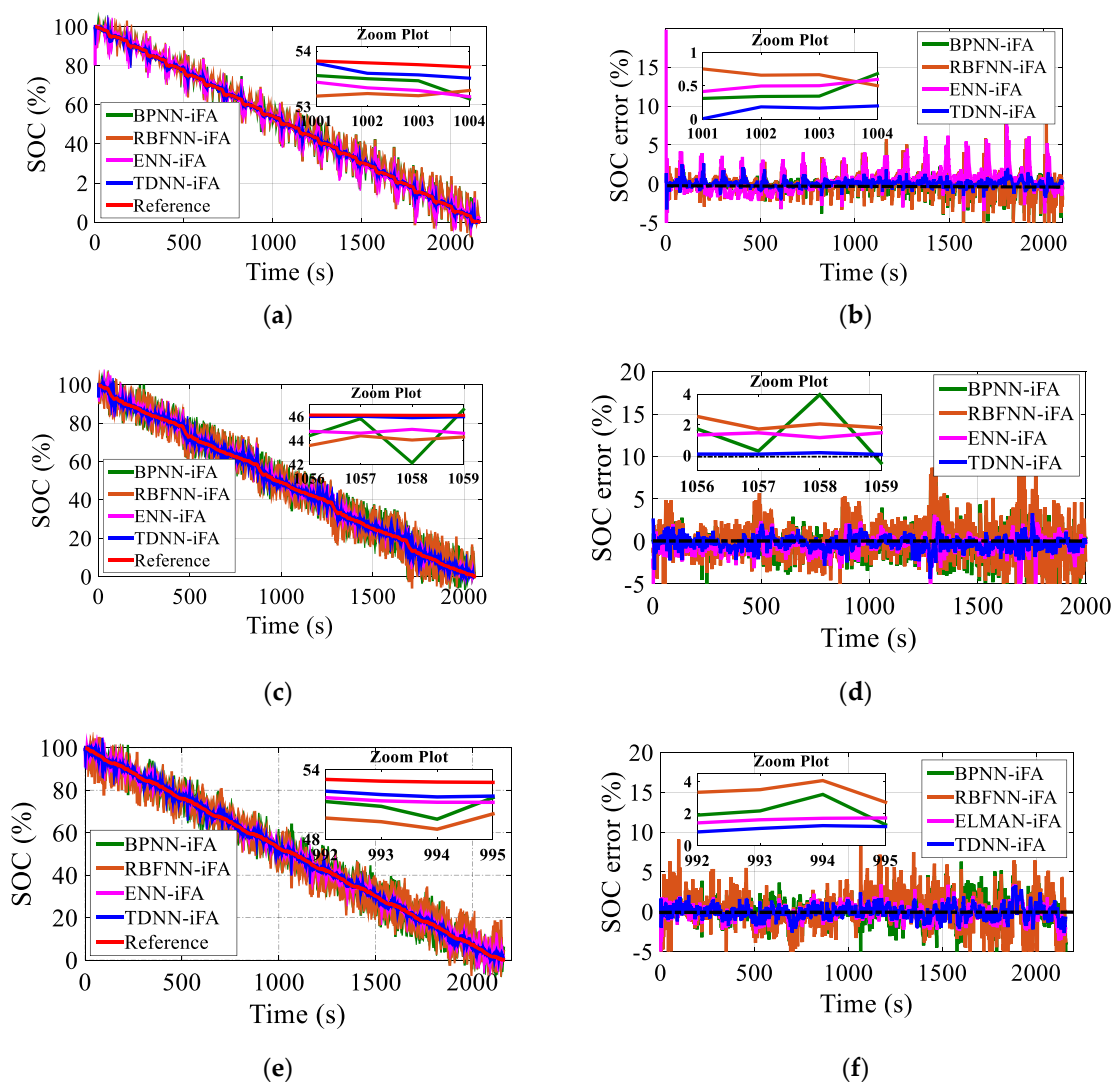


Figure 13. SOC and SOC error estimation results: (a,b) DST, (c,d) FUDS, and (e,f) US06 at $25\text{ }^{\circ}\text{C}$.

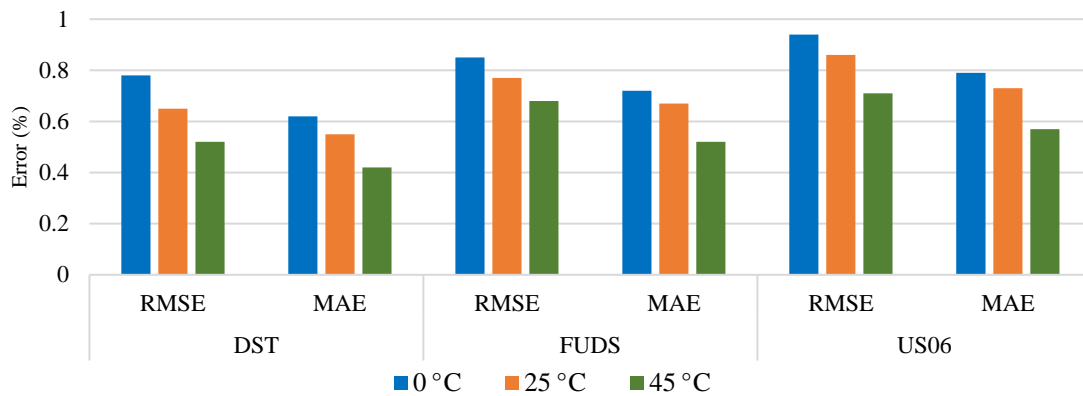


Figure 14. SOC performance comparison under different temperatures and EV drive cycles.

5.4. SOC Robustness Validation against Noise Effects

The robustness of the iFA-based TDNN algorithm for SOC estimation is validated against both bias noise and random noise, as presented in Figure 15 and Table 5. The results reveal that the combination of bias and random noise has a small influence on SOC estimation with regard to RMSE, MAE, and SOC error. It is noticed that the addition of bias and random noises elevates the SOC error bound a bit; however, SOC error rates have stayed inside the reasonable range. For example, iFA-based TDNN achieves the maximum SOC error of 3.5% and 5.8% in SDT and HPPC load profiles, respectively, for the LiNMC battery. In line with that, the proposed method obtains RMSE of 0.558% and 1.112%, respectively. The results are also satisfactory in the LiNCA battery, where the maximum SOC error is reported to be 4% and 6.3% in SDT and HPPC tests, respectively. The aforementioned results prove that the iFA-based TDNN algorithm demonstrates strong robustness against biased noises and random noises toward accurate SOC estimation.

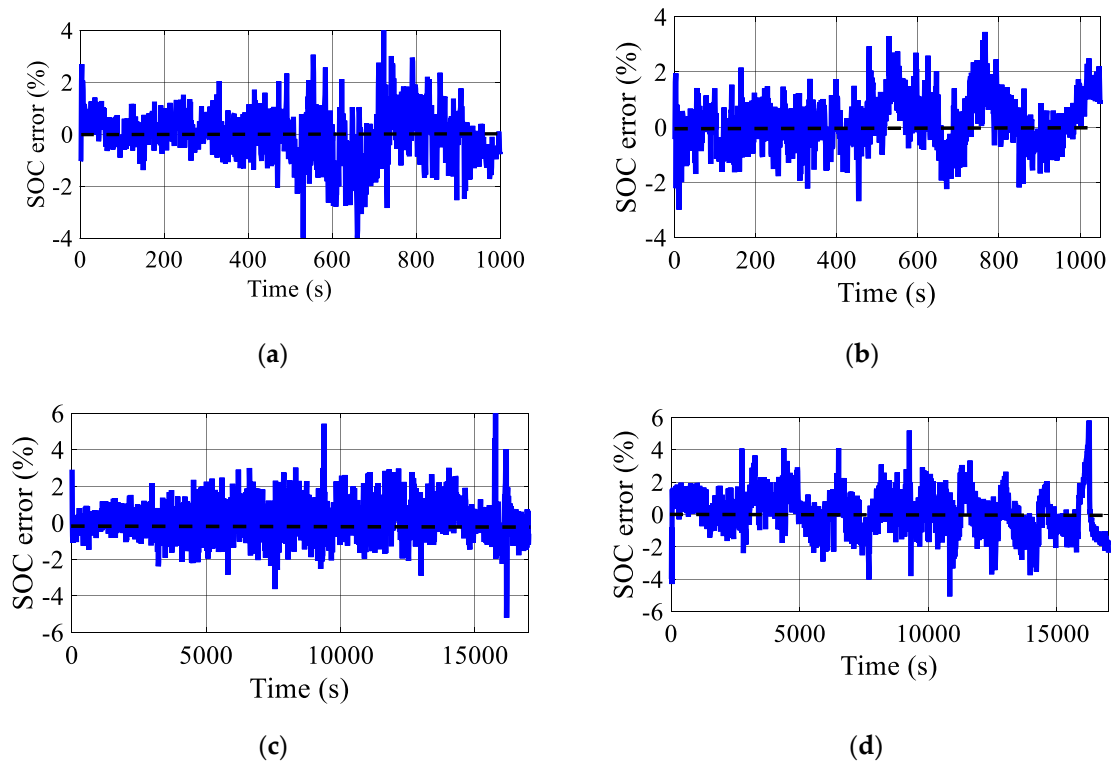


Figure 15. SOC error analysis at 0.01 V/0.1 A bias noise and 0.01 V/ 0.1 A random noise: (a) SDT for the LiNCA battery; (b) SDT for the LiNMC battery; (c) HPPC for the LiNCA battery; and (d) HPPC for the LiNMC battery.

Table 5. SOC estimation with noise effect under SDT and HPPC tests.

Test	Battery	0.01 V/0.1 A Bias Noise and 0.01 V/0.1 A Random Noise		
		RMSE (%)	MAE (%)	SOC Error (%)
SDT	LiNCA	0.765	0.482	[−3.9, 4]
	LiNMC	0.558	0.386	[−2.9, 3.5]
HPPC	LiNCA	1.287	0.852	[−5.2, 6.3]
	LiNMC	1.112	0.728	[−5.1, 5.8]

5.5. SOC Robustness Validation against Aging Impacts

The comparative performance between LiNCA and LiNMC batteries is further examined using the aging cycle test. The current and voltage characteristics of LiNCA and LiNMC batteries for one aging cycle are shown in Figure 16.

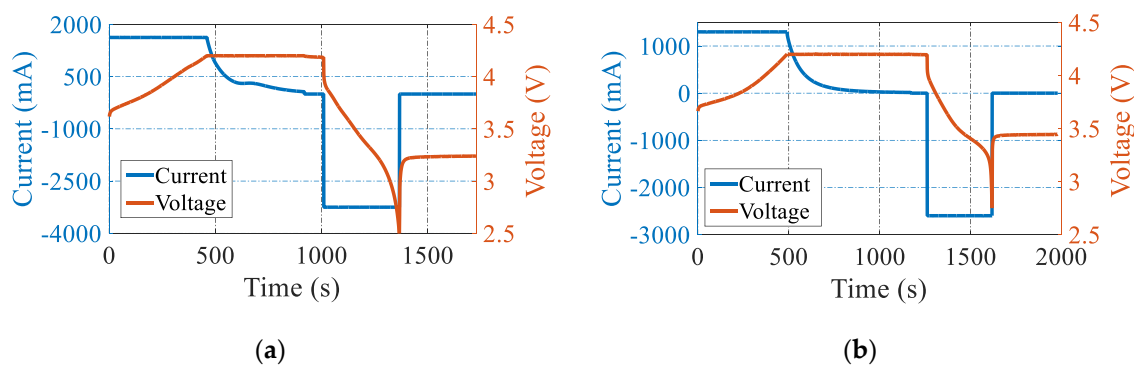


Figure 16. One aging cycle test: (a) the LiNCA battery and (b) the LiNMC battery.

The performance degradation of LiNCA and LiNMC batteries is assessed using discharge capacity and cycle life under four milestone aging cycles; 50 cycles, 100 cycles, 150 cycles, and 200 cycles, as depicted in Table 6. The discharge capacity denotes the current capacity of the lithium-ion battery after certain aging cycles while cycle life compares the present capacity of an aged battery cell with the capacity of a new battery cell. The results indicate that the capacity of LiNCA falls faster than LiNMC battery, which means LiNCA performs poorly under many aging cycles. In contrast, LiNMC shows strong adaptability and robustness against many aging cycles. For instance, the LiNCA battery has a capacity of 2763 mAh after 200 aging cycles, which is reduced by 9.5% in comparison to the value obtained after 50 aging cycles. However, only a 3.6% decrease in capacity is noted in the LiNMC battery. The results of the cycle life are also satisfactory in the LiNMC battery under many aging cycles. For example, LiNMC has a cycle life of 95.756% after 200 aging cycles; nevertheless, the cycle life of LiNCA is reduced quickly and estimated to be 85.923%.

Table 6. Battery performance degradation in the LiNCA battery and LiNMC battery.

Aging Cycles	Battery	Discharge Capacity (mAh)	Cycle Life (%)
50	LiNCA	3052	95.107
	LiNMC	2515	97.889
100	LiNCA	2951	91.282
	LiNMC	2477	97.231
150	LiNCA	2850	88.629
	LiNMC	2460	96.931
200	LiNCA	2763	85.923
	LiNMC	2425	95.756

At first, the LiNCA and LiNMC batteries are cycled for a definite number of cycles. After the completion of the aging cycle test, the lithium-ion battery is loaded with the HPPC test. The performance of the TDNN-iFA model is tested with the HPPC experimental dataset of aged LiNCA and LiNMC batteries for 50, 100, 150, and 200 cycles. The results of SOC and SOC errors under 50, 100, 150, and 200 aging cycles for LiNCA and LiNMC battery are presented in Figures 17 and 18, respectively. Moreover, the results of the RMSE, MAE, and SOC error bound are depicted in Table 7.

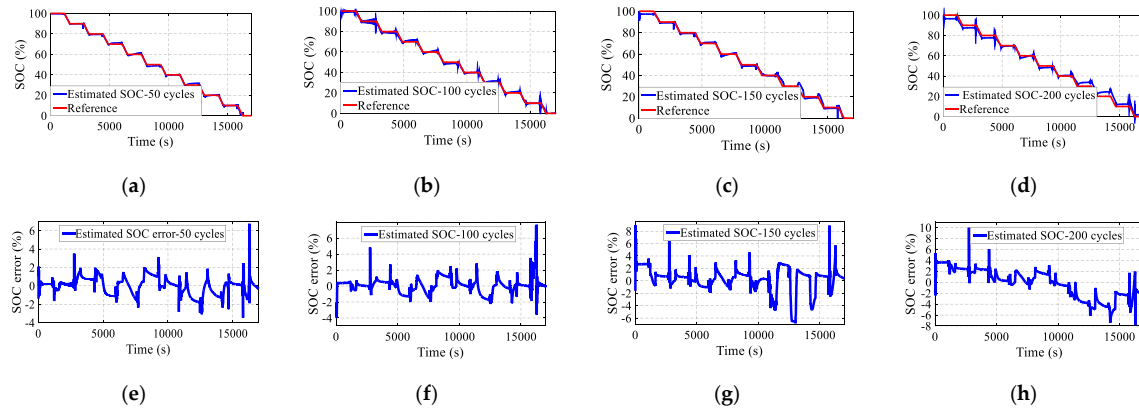


Figure 17. Aging performance for the LiNCA battery: (a) SOC estimation under 50 cycles, (b) SOC estimation under 100 cycles, (c) SOC estimation under 150 cycles, and (d) SOC estimation under 200 cycles; (e) SOC error under 50 cycles, (f) SOC error under 100 cycles, (g) SOC error under 150 cycles, and (h) SOC error under 200 cycles.

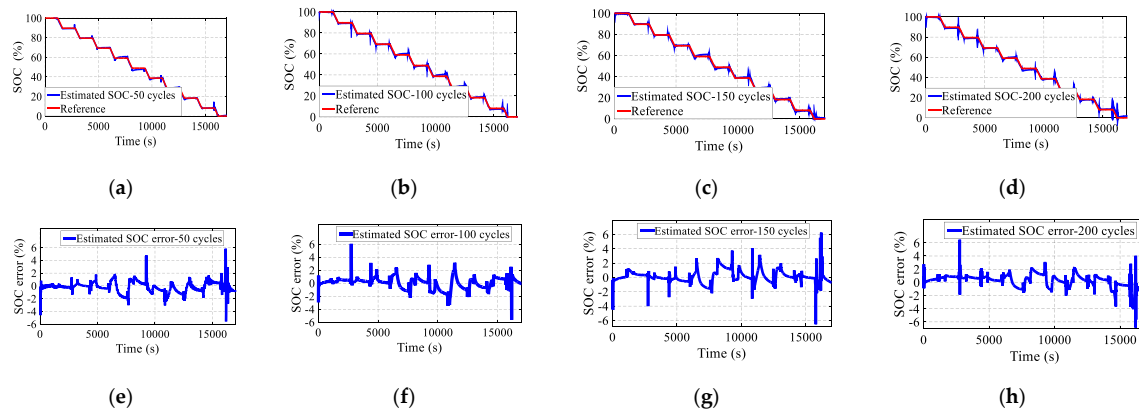


Figure 18. Aging performance for the LiNMC battery: (a) SOC estimation under 50 cycles, (b) SOC estimation under 100 cycles, (c) SOC estimation under 150 cycles, and (d) SOC estimation under 200 cycles; (e) SOC error under 50 cycles, (f) SOC error under 100 cycles, (g) SOC error under 150 cycles, and (h) SOC error under 200 cycles.

Table 7. Performance assessment of LiNCA and LiNMC batteries under aging cycles.

Aging Cycles	Battery	RMSE (%)	MAE (%)	SOC Error (%)
50	LiNCA	0.933	0.717	[−3.4, 6.7]
	LiNMC	0.821	0.623	[−5.5, 5.7]
100	LiNCA	1.525	0.923	[−3.6, 7.6]
	LiNMC	0.864	0.685	[−5.8, 6]
150	LiNCA	1.878	1.338	[−6.8, 8.8]
	LiNMC	0.927	0.742	[−6.5, 6.2]
200	LiNCA	2.614	1.785	[−7.8, 9.9]
	LiNMC	1.046	0.825	[−6.7, 6.4]

It is observed that the LiNCA battery has higher error rates than the LiNMC battery. For instance, at 50 aging cycles, the LiNCA battery has RMSE of 0.933%, while this is 0.821% in the LiNMC battery. A similar type of results is also noticed in the MAE and SOC error rates. Moreover, the SOC error range is found to be $[-3.4\%, 6.7\%]$ in the LiNCA battery, while that for LiNMC is $[-5.5\%, 5.7\%]$. SOC error rates move up as the aging cycle increases from 50 to 100. For example, in the LiNMC battery, the MAE is calculated to be 0.685% at 100 cycles, while it is 0.623% at 50 cycles. Under 100 aging cycles, the LiNMC battery delivers better solutions than the LiNCA battery, achieving a maximum SOC error and RMSE of 6% and 0.864%, respectively. The assessment of iFA-based TDNN algorithm for SOC estimation is further conducted under 150 aging cycles for LiNCA and LiNMC batteries. The results show that the proposed model tracks the reference SOC precisely for both the LiNCA battery and LiNMC battery. Like previous aging cycles, the LiNMC battery is also dominant over the LiNCA battery in providing a low error rate. The LiNCA battery has a SOC error range of $[-6.8\%, 8.8\%]$ while that for LiNMC is $[-6.5\%, 6.2\%]$. Besides, the LiNMC battery obtains low RMSE and MAE, indicating 0.927% and 0.742%, respectively.

The SOC evaluation of the LiNCA battery and LiNMC battery is further verified under 200 aging cycles. It is observed that the accuracy of the LiNCA battery drops significantly when it is deeply cycled. The results indicate that SOC error range and RMSE is attained to be $[-7.8\%, 9.9\%]$, and 2.614% respectively, for the LiNCA battery. However, the LiNMC battery delivers outstanding SOC estimation results under 200 aging cycles, with a SOC error limit and RMSE of $[-6.7\%, 6.4\%]$, and 1.046%, respectively.

To test the LiNCA and LiNMC batteries at a higher number of cycles, the verification of SOC estimation by the proposed algorithm is carried out under 400 and 600 cycles. The results indicate that the cycle life of LiNCA and LiNMC batteries under 400 cycles is 73.685% and 91.597%, respectively. It is reported in the literature that a lithium-ion battery with a cycle life below 80% is declared unsafe and unserviceable [37]. In this regard, LiNCA batteries are no longer usable, and accordingly a replacement is needed. In contrast, the LiNMC battery has a cycle life well above 80% and hence is used for algorithm validation and analysis. At 400 aging cycles, the LiNMC battery achieves RMSE and MAE of 1.327% and 1.128%, which are raised by 21.2% and 26.8%, respectively, compared to the values obtained under 200 aging cycles. Moreover, the LiNMC battery illustrates satisfactory performance under 600 aging cycles, indicating cycle life, RMSE, and MAE values of 88.257%, 1.582%, and 1.368%, respectively. These results show that LiNCA batteries are not appropriate for a high number of aging cycles above 400. Nevertheless, LiNMC batteries are outstanding even if the aging cycles increase to 600, demonstrating high adaptability and robustness for EV operation.

5.6. Comparative Validation with the Existing Methods

Apart from data-driven techniques for SOC validation, the accuracy of the proposed optimized TDNN algorithm is compared with the traditional methods and model-based approaches including OCV, CC, KF, PF, H_∞ filter, recursive least square (RLS), and observers, as illustrated in Table 8.

The key implementation factors associated with SOC estimation such as lithium-ion battery chemistry, battery capacity, changing temperature, and validation profiles are taken into consideration to conduct the comparative analysis. The SOC error rates are assessed under a similar type of validation profile to carry out a fair comparative study. For instance, in 1 Coulomb (C) SDT, the proposed method computes MAE of 0.2374% and 0.1452% in the LiNCA battery and LiNMC battery, respectively. Nevertheless, the MAE is found to be more than 2% in unscented Kalman filter (UKF) and H_∞ Filter methods under the same load profile. The performance of the iFA-based TDNN for SOC estimation is further examined using different EV drive cycles. It is observed that RMSE is reported below 1% in the proposed algorithm under different EV drive cycles, while that for OCV, the unscented particle filter (UPF), RLS, and proportional integral observer (PIO) is above 1%. In summary, the iFA-based TDNN algorithm has proven to be excellent in terms of accuracy, adaptability, and robustness compared to the existing notable SOC estimation techniques.

Table 8. Comparative performance analysis between the proposed method and the existing methods.

Ref.	Method	Battery Chemistry	Temperature	Experimental Validation Profile	Error Rate
[38]	OCV	1.1 Ah LiFePO ₄	0 °C to 50 °C at an interval of 10 °C	DST, FUDS	RMSE 5%
[39]	CC	2.3 Ah Lithium-ion cell	Room temperature	C-rates Charging-discharging current	MAE 1.905%
[40]	UKF	24 Ah LiNMC	Room temperature at 25 °C ± 2 °C	1 C SDT	MAE 2.56%
[41]	H _∞ Filter	2.4 Ah Lithium-ion cell	Constant temperature	1 C SDT	Max SOC error 5.36%
[42]	UPF	10 Ah LiFePO ₄	−20 °C–50 °C	EV operation condition	MAE 3.96%
[43]	RLS	90 Ah LiFePO ₄	−10 °C–50 °C	Urban EV drive cycle	RMSE 2.05%
[44]	SMO	5 Ah Lithium polymer battery	Room temperature	1 C SDT	MAE 1.8%
[45]	PIO	90 Ah Lithium-ion cells	0 °C, 25 °C, 40 °C	DST	RMSE 1.2%
		3.2 Ah LiNCA	Room Temperature	1 C SDT, HPPC	MAE 0.2374% (SDT)
	Proposed Method	2.6 Ah LiNMC			MAE 0.4612% (HPPC)
		2.0 Ah LiNCA	0 °C, 25 °C, 45 °C	DST, FUDS, US06	MAE 0.1452% (SDT)
					MAE 0.3283% (HPPC)
					RMSE < 1%
					MAE < 0.8%

6. Conclusions

An improved data-driven algorithm using TDNN optimized by iFA is proposed to achieve accurate SOC estimation of lithium-ion batteries. The iFA algorithm improves the computational capability of TDNN by choosing the optimum values of UTD and HNs, thus leading to an enhancement in SOC accuracy and robustness. For the verification, the fully developed algorithm is examined with two types of lithium-ion battery cells under two different experiments, namely SDT and HPPC. The TDNN-iFA algorithm achieves excellent SOC estimation results with low RMSE, SD, MSE, MAPE, and MAE, while having a narrow SOC error below 5% in the SDT and HPPC tests. The SOC estimation results under EV drive cycles and variable temperatures also prove the dominance of the iFA-based TDNN algorithm where RMSE is reported under 1%. Besides, the reasonable accuracy under noise and aging impacts illustrates the adaptability and robustness of the TDNN-iFA algorithm against uncertainties. Furthermore, detailed comparative analysis with the existing SOC estimation techniques considering different loads and temperatures demonstrates that the developed optimized data-driven method can provide excellent solutions with respect to the accuracy, efficiency, and robustness. The key information, results, and analysis achieved from this study would be important for the EV automobile industry toward the development of an enhanced SOC estimation approach. Hence, further investigation of SOC estimation via the optimized TDNN method will not only increase the battery life cycle but also confirm a reliable operation of EVs, resulting in a substantial growth of the EV market. Future research work should include the validation of iFA-based TDNN algorithm for SOC estimation of the lithium-ion battery pack in EV applications.

Author Contributions: Conceptualization, M.S.H.L. and M.A.H.; methodology, M.S.H.L.; software, M.S.H.L.; validation, M.S.H.L.; formal analysis, M.S.H.L.; investigation, M.S.H.L. and M.A.H.; resources, M.A.H. and A.H.; data curation, M.S.H.L.; writing—original draft, M.S.H.L.; writing—review and editing, M.A.H., A.H., A.A., M.H.M.S. and K.M.M.; visualization, M.S.H.L.; supervision, M.A.H., A.H., A.A. and M.H.M.S.; project administration, M.A.H.; funding acquisition, M.S.H.L. and M.A.H. All authors have read and agreed to the published version of the manuscript.

Funding: This work was supported by Universiti Kebangsaan Malaysia under Grant LRGS/2018/UNITEN-UKM/EWS/04.

Conflicts of Interest: The authors declare no conflict of interest.

References

- Mongird, K.; Viswanathan, V.; Balducci, P.; Alam, J.; Fotedar, V.; Koritarov, V.; Hadjerioua, B. An Evaluation of Energy Storage Cost and Performance Characteristics. *Energies* **2020**, *13*, 3307. [[CrossRef](#)]
- Stampatori, D.; Raimondi, P.P.; Noussan, M. Li-Ion Batteries: A Review of a Key Technology for Transport Decarbonization. *Energies* **2020**, *13*, 2638. [[CrossRef](#)]

3. Huang, B.; Pan, Z.; Su, X.; An, L. Recycling of lithium-ion batteries: Recent advances and perspectives. *J. Power Sources* **2018**, *399*, 274–286. [\[CrossRef\]](#)
4. Yuan, W.-P.; Jeong, S.-M.; Sean, W.-Y.; Chiang, Y.-H. Development of Enhancing Battery Management for Reusing Automotive Lithium-Ion Battery. *Energies* **2020**, *13*, 3306. [\[CrossRef\]](#)
5. Balasingam, B.; Ahmed, M.; Pattipati, K. Battery Management Systems—Challenges and Some Solutions. *Energies* **2020**, *13*, 2825. [\[CrossRef\]](#)
6. Zhang, R.; Xia, B.; Li, B.; Cao, L.; Lai, Y.; Zheng, W.; Wang, H.; Wang, W.; Zhang, R.; Xia, B.; et al. State of the Art of Lithium-Ion Battery SOC Estimation for Electrical Vehicles. *Energies* **2018**, *11*, 1820. [\[CrossRef\]](#)
7. Hussain, S.; Nengroo, S.H.; Zafar, A.; Kim, H.-J.; Alvi, M.J.; Ali, M.U. Towards a Smarter Battery Management System for Electric Vehicle Applications: A Critical Review of Lithium-Ion Battery State of Charge Estimation. *Energies* **2019**, *12*, 446.
8. Hu, X.; Feng, F.; Liu, K.; Zhang, L.; Xie, J.; Liu, B. State estimation for advanced battery management: Key challenges and future trends. *Renew. Sustain. Energy Rev.* **2019**, *114*, 109334. [\[CrossRef\]](#)
9. Zhang, Y.; Song, W.; Lin, S.; Feng, Z. A novel model of the initial state of charge estimation for LiFePO 4 batteries. *J. Power Sources* **2014**, *248*, 1028–1033. [\[CrossRef\]](#)
10. Antonucci, V.; Artale, G.; Brunaccini, G.; Caravello, G.; Cataliotti, A.; Cosentino, V.; Di Cara, D.; Ferraro, M.; Guaiana, S.; Panzavecchia, N.; et al. Li-ion Battery Modeling and State of Charge Estimation Method Including the Hysteresis Effect. *Electronics* **2019**, *8*, 1324. [\[CrossRef\]](#)
11. Lai, X.; Yi, W.; Zheng, Y.; Zhou, L. An All-Region State-of-Charge Estimator Based on Global Particle Swarm Optimization and Improved Extended Kalman Filter for Lithium-Ion Batteries. *Electronics* **2018**, *7*, 321. [\[CrossRef\]](#)
12. Yang, F.; Xing, Y.; Wang, D.; Tsui, K.L. A comparative study of three model-based algorithms for estimating state-of-charge of lithium-ion batteries under a new combined dynamic loading profile. *Appl. Energy* **2016**, *164*, 387–399. [\[CrossRef\]](#)
13. Xiong, R.; Zhang, Y.; He, H.; Zhou, X.; Pecht, M.G. A Double-Scale, Particle-Filtering, Energy State Prediction Algorithm for Lithium-Ion Batteries. *IEEE Trans. Ind. Electron.* **2018**, *65*, 1526–1538. [\[CrossRef\]](#)
14. Liu, C.Z.; Zhu, Q.; Li, L.; Liu, W.Q.; Wang, L.Y.; Xiong, N.; Wang, X.Y. A State of Charge Estimation Method Based on H_∞ Observer for Switched Systems of Lithium-Ion Nickel-Manganese-Cobalt Batteries. *IEEE Trans. Ind. Electron.* **2017**, *64*, 8128–8137. [\[CrossRef\]](#)
15. Du, J.; Liu, Z.; Wang, Y.; Wen, C. An adaptive sliding mode observer for lithium-ion battery state of charge and state of health estimation in electric vehicles. *Control Eng. Pract.* **2016**, *54*, 81–90. [\[CrossRef\]](#)
16. Rivera-Barrera, J.; Muñoz-Galeano, N.; Sarmiento-Maldonado, H. SoC Estimation for Lithium-ion Batteries: Review and Future Challenges. *Electronics* **2017**, *6*, 102. [\[CrossRef\]](#)
17. He, W.; Williard, N.; Chen, C.; Pecht, M. State of charge estimation for Li-ion batteries using neural network modeling and unscented Kalman filter-based error cancellation. *Int. J. Electr. Power Energy Syst.* **2014**, *62*, 783–791. [\[CrossRef\]](#)
18. Haddad Zarif, M.; Charkhgard, M.; Alfi, A. Hybrid state of charge estimation for lithium-ion batteries: Design and implementation. *IET Power Electron.* **2014**, *7*, 2758–2764.
19. Lipu, M.S.H.; Hannan, M.A.; Hussain, A.; Saad, M.H.M.; Ayob, A.; Uddin, M. Extreme Learning Machine Model for State of Charge Estimation of Lithium-ion battery Using Gravitational Search Algorithm. *IEEE Trans. Ind. Appl.* **2019**, *55*, 4225–4234. [\[CrossRef\]](#)
20. Cui, D.; Xia, B.; Zhang, R.; Sun, Z.; Lao, Z.; Wang, W.; Sun, W.; Lai, Y.; Wang, M.; Cui, D.; et al. A Novel Intelligent Method for the State of Charge Estimation of Lithium-Ion Batteries Using a Discrete Wavelet Transform-Based Wavelet Neural Network. *Energies* **2018**, *11*, 995. [\[CrossRef\]](#)
21. Liu, K.; Li, Y.; Hu, X.; Lucu, M.; Widanage, W.D. Gaussian Process Regression with Automatic Relevance Determination Kernel for Calendar Aging Prediction of Lithium-Ion Batteries. *IEEE Trans. Ind. Inform.* **2020**, *16*, 3767–3777. [\[CrossRef\]](#)
22. Lipu, M.S.H.; Hannan, M.A.; Hussain, A.; Saad, M.H.M.; Ayob, A.; Blaabjerg, F. State of Charge Estimation for Lithium-ion Battery Using Recurrent NARX Neural Network Model Based Lighting Search Algorithm. *IEEE Access* **2018**, *6*, 28150–28161. [\[CrossRef\]](#)
23. Bian, C.; He, H.; Yang, S. Stacked bidirectional long short-term memory networks for state-of-charge estimation of lithium-ion batteries. *Energy* **2020**, *191*, 116538. [\[CrossRef\]](#)
24. Xiao, B.; Liu, Y.; Xiao, B. Accurate state-of-charge estimation approach for lithium-ion batteries by gated recurrent unit with ensemble optimizer. *IEEE Access* **2019**, *7*, 54192–54202. [\[CrossRef\]](#)

25. Awadallah, M.A.; Venkatesh, B. Accuracy improvement of SOC estimation in lithium-ion batteries. *J. Energy Storage* **2016**, *6*, 95–104. [[CrossRef](#)]
26. Chaoui, H.; Ibe-Ekeocha, C.C.; Gualous, H. Aging prediction and state of charge estimation of a LiFePO₄ battery using input time-delayed neural networks. *Electr. Power Syst. Res.* **2017**, *146*, 189–197. [[CrossRef](#)]
27. Shao, Y.E.; Lin, S.-C. Using a Time Delay Neural Network Approach to Diagnose the Out-of-Control Signals for a Multivariate Normal Process with Variance Shifts. *Mathematics* **2019**, *7*, 959. [[CrossRef](#)]
28. Hannan, M.A.; Lipu, M.S.H.; Hussain, A.; Saad, M.H.; Ayob, A. Neural Network Approach for Estimating State of Charge of Lithium-ion Battery Using Backtracking Search Algorithm. *IEEE Access* **2018**, *6*, 10069–10079. [[CrossRef](#)]
29. Hagan, M.T.; Menhaj, M.B. Training feedforward networks with the Marquardt algorithm. *IEEE Trans. Neural Netw.* **1994**, *5*, 989–993. [[CrossRef](#)] [[PubMed](#)]
30. Lv, C.; Xing, Y.; Zhang, J.; Na, X.; Li, Y.; Liu, T.; Cao, D.; Wang, F.-Y. Levenberg–Marquardt Backpropagation Training of Multilayer Neural Networks for State Estimation of a Safety-Critical Cyber-Physical System. *IEEE Trans. Ind. Inform.* **2018**, *14*, 3436–3446. [[CrossRef](#)]
31. Xia, X.; Gui, L.; He, G.; Xie, C.; Wei, B.; Xing, Y.; Wu, R.; Tang, Y. A hybrid optimizer based on firefly algorithm and particle swarm optimization algorithm. *J. Comput. Sci.* **2018**, *26*, 488–500. [[CrossRef](#)]
32. Xu, S.S.-D.; Huang, H.-C.; Kung, Y.-C.; Lin, S.-K. Collision-Free Fuzzy Formation Control of Swarm Robotic Cyber-Physical Systems Using a Robust Orthogonal Firefly Algorithm. *IEEE Access* **2019**, *7*, 9205–9214. [[CrossRef](#)]
33. Ball, A.K.; Roy, S.S.; Kisku, D.R.; Murmu, N.C.; Dos Santos Coelho, L. Optimization of drop ejection frequency in EHD inkjet printing system using an improved Firefly Algorithm. *Appl. Soft Comput. J.* **2020**, *94*, 106438. [[CrossRef](#)]
34. Wang, Y.; Zhang, C.; Chen, Z. A method for joint estimation of state-of-charge and available energy of LiFePO₄batteries. *Appl. Energy* **2014**, *135*, 81–87. [[CrossRef](#)]
35. Hannan, M.A.; Lipu, M.S.H.; Hussain, A.; Ker, P.J.; Mahlia, T.M.I.; Mansor, M.; Ayob, A.; Saad, M.H.; Dong, Z.Y. Toward Enhanced State of Charge Estimation of Lithium-ion Batteries Using Optimized Machine Learning Techniques. *Sci. Rep.* **2020**, *10*, 4687. [[CrossRef](#)]
36. CALCE. Lithium-ion Battery Experimental Data. Available online: <https://web.calce.umd.edu/batteries/data.htm> (accessed on 23 August 2018).
37. Naha, A.; Han, S.; Agarwal, S.; Guha, A.; Khandelwal, A.; Tagade, P.; Hariharan, K.S.; Kolake, S.M.; Yoon, J.; Oh, B. An Incremental Voltage Difference Based Technique for Online State of Health Estimation of Li-ion Batteries. *Sci. Rep.* **2020**, *10*, 9526. [[CrossRef](#)] [[PubMed](#)]
38. Xing, Y.; He, W.; Pecht, M.; Tsui, K.L. State of charge estimation of lithium-ion batteries using the open-circuit voltage at various ambient temperatures. *Appl. Energy* **2014**, *113*, 106–115. [[CrossRef](#)]
39. Wu, T.-H.; Moo, C.-S.; Wu, T.-H.; Moo, C.-S. State-of-Charge Estimation with State-of-Health Calibration for Lithium-Ion Batteries. *Energies* **2017**, *10*, 987.
40. Chen, Y.; Huang, D.; Zhu, Q.; Liu, W.; Liu, C.; Xiong, N. A new state of charge estimation algorithm for lithium-ion batteries based on the fractional unscented kalman filter. *Energies* **2017**, *10*, 1313. [[CrossRef](#)]
41. Zhu, Q.; Xiong, N.; Yang, M.L.; Huang, R.S.; Hu, G. Di State of charge estimation for lithium-ion battery based on nonlinear observer: An H_{∞} method. *Energies* **2017**, *10*, 679. [[CrossRef](#)]
42. He, Y.; Liu, X.; Zhang, C.; Chen, Z. A new model for State-of-Charge (SOC) estimation for high-power Li-ion batteries. *Appl. Energy* **2013**, *101*, 808–814. [[CrossRef](#)]
43. Duong, V.H.; Bastawrous, H.A.; See, K.W. Accurate approach to the temperature effect on state of charge estimation in the LiFePO₄ battery under dynamic load operation. *Appl. Energy* **2017**, *204*, 560–571. [[CrossRef](#)]
44. Chen, X.; Shen, W.; Cao, Z.; Kapoor, A. A novel approach for state of charge estimation based on adaptive switching gain sliding mode observer in electric vehicles. *J. Power Sources* **2014**, *246*, 667–678. [[CrossRef](#)]
45. Zheng, L.; Zhang, L.; Zhu, J.; Wang, G.; Jiang, J. Co-estimation of state-of-charge, capacity and resistance for lithium-ion batteries based on a high-fidelity electrochemical model. *Appl. Energy* **2016**, *180*, 424–434. [[CrossRef](#)]

